

February 1998

HUB-EP-98/10

JINR E2-98-27

Gluon propagator and zero-momentum modes in SU(2) lattice gauge theory

G. Damm ^a, W. Kerler ^{a,b}, V.K. Mitrjushkin ^c

^a *Fachbereich Physik, Universität Marburg, D-35032 Marburg, Germany*

^b *Institut für Physik, Humboldt-Universität, D-10115 Berlin, Germany*

^c *Joint Institute for Nuclear Research, Dubna, Russia*

Abstract

We investigate propagators in Lorentz (or Landau) gauge by Monte Carlo simulations. In order to be able to compare with perturbative calculations we use large β values. There the breaking of the $Z(2)$ symmetry turns out to be important for all of the four lattice directions. Therefore we make sure that the analysis is performed in the correct state. We discuss implications of the gauge fixing mechanism and point out the form of the weak-coupling behavior to be expected in the presence of zero-momentum modes. Our numerical result is that the gluon propagator in the weak-coupling limit is strongly affected by zero-momentum modes. This is corroborated in detail by our quantitative comparison with analytical calculations.

1. Introduction

Fundamental results on QCD have been obtained in continuum perturbation theory as well as nonperturbatively on the lattice. It appears important to connect the knowledge from these two approaches more closely. Progress within this respect is expected from the calculations of typical quantities of perturbation theory by Monte Carlo simulations in lattice gauge theory. The gluon propagator is a fundamental quantity for such an investigation.

In the seminal paper by Mandula and Ogilvie [1] the zero-momentum gluon propagator $\Gamma(\tau) = \Gamma(\tau; \vec{p} = \vec{0})$ has been numerically calculated in the Lorentz (or Landau) gauge. The analysis of the τ -dependence of this propagator drove the authors of [1] to the conclusion that $\Gamma(\tau)$ is consistent with the propagation of a massive gluon. Therefore, the effect of dynamical mass generation was declared to be observed. Since that there was quite a number of papers devoted to the calculation and analysis of gauge-variant zero-momentum propagators at zero and nonzero temperatures following the same line as paper [1] (see, e.g. [2–8]) However, the impact of zero-momentum modes on the propagators has not been analyzed.

Recently it has been shown by one of us that zero-momentum modes may strongly affect some gauge-dependent correlators [9]. In some cases, e.g., in the Coulomb phase in pure $U(1)$ gauge theory, zero-momentum modes can mimic the effective masses defined in a standard way (see eq. (5.2)). This is apparent from the data of [10]. Because so far nothing is known about the magnitude of this effect in nonabelian gauge theory, it appears highly desirable to perform simulations which clarify this issue. In order to be able to compare quantitatively with perturbative calculations and to draw firm conclusions it is reasonable to begin this study in the truly perturbative region, i.e. at large values of β .

In the present paper we perform Monte Carlo simulations in pure $SU(2)$ gauge theory in the four-dimensional volume $V_4 = L_1 L_2 L_3 L_4$ with periodic boundary conditions. We use the Wilson action

$$S = \beta \sum_P \left(1 - \frac{1}{2} \text{Tr } U_P \right), \quad (1.1)$$

and the Lorentz gauge as described in Section 2. We discuss the working of the gauge fixing mechanism in detail and present analytical forms of the propagators appropriate at weak-coupling in the presence of zero-momentum modes. We demonstrate the effects of the broken $Z(2)$ symmetry and show that in the appropriate $Z(2)$ state there is agreement with perturbative calculations. In particular, we find that there is a sizable effect caused by zero-momentum modes which can be understood quantitatively.

2. Gauge fixing procedure

In $SU(2)$ lattice gauge theory the Lorentz gauge is fixed by maximizing

$$F = \frac{1}{4V_4} \sum_{\mu,x} \text{Tr } U_{\mu x} \quad (2.1)$$

by appropriate gauge transformations $U_{\mu x} \rightarrow V_{x+e_\mu} U_{\mu x} V_x^\dagger$, which implies the local condition

$$\sum_{\mu} \bar{\partial}_{\mu} U_{\mu x} = 0 \quad (2.2)$$

(where $\bar{\partial}_{\mu} f(x) = f(x) - f(x - e_{\mu})$). The maximized functional (2.1) may be cast into the form

$$F_{\text{max}} = \frac{1}{8V_4} \sum_x \text{Tr } (M_x V_x^\dagger) \quad (2.3)$$

where

$$M_x = \sum_{\mu} (V_{x+e_{\mu}} U_{\mu x} + V_{x-e_{\mu}} U_{\mu, x-e_{\mu}}^\dagger) \quad (2.4)$$

From the fact that (2.3) is maximal it follows that the maximizing gauge transformations are given by

$$V_x = M_x / \|M_x\| \quad (2.5)$$

where $\|M_x\|^2 = \frac{1}{2} \text{Tr}(M_x M_x^\dagger)$. Obviously (2.5), is a system of equations which determines all V 's given the U 's of the configuration. (It should not to be mixed up with the relation without V 's on the r.h.s. and with the U 's being the ones of the

particular iteration step, which is used iteratively site by site in numerical gauge fixing).

The gauge-fixing procedure is based on the equality $\langle P \rangle_f = \langle P^V \rangle$ of the expectation with gauge fixing for the observable P to that without gauge fixing for the transformed observable P^V . We note that this actually amounts to switching to the gauge-invariant observable P_{eff} which is related to the gauge-variant one P in the gauge under consideration, i.e. that $P_{\text{eff}} = P^V$. The respective general relation $\langle P \rangle_f = \langle P_{\text{eff}} \rangle$ with $P_{\text{eff}} = \int_V \mathcal{F} P / \int_V \mathcal{F}$, where \mathcal{F} is a general gauge fixing function, has been pointed out some time ago [11].

It should be realized that the mechanism leading from a gauge-variant observable P to an effectively gauge-invariant one P_{eff} is simple. The gauge-fixing function provides strings of gauge fields which can combine with the given gauge-variant operators to gauge-invariant objects (and, of course, only such objects contribute to the integrals). For example, given a gauge field at a certain link, a string may be provided such that one gets a loop which contains this link. In practice there can be many suitable strings such that one arrives at a sum of gauge-invariant terms.

In the present case the gauge-invariant observables can be constructed. To see this one has to realize that after maximization the original U variables due to the gauge transformation are decorated by V factors. On the other hand, these V factors are given here by (2.5), which therefore can be used to eliminate the V 's successively from P^V . In detail, one replaces a V by (2.5) which introduces next V 's from the r.h.s of (2.5), then replaces these V 's again by (2.5), and so on. This procedure terminates when all V 's are eliminated and one has arrived at an expression which contains only closed loops of gauge fields U .

In the gauge-invariant observable thus obtained there are loops which include the gauge-variant parts of the gauge-variant observable P according to the mechanism explained above. Furthermore, noting that the factors $\|M_x\|$ in (2.5) also contain V 's, it becomes obvious that the terms of the effectively invariant observable are multiplied by weights which stem from these $\|M_x\|$ factors and which only depend on gauge-field loops (the locations of which are not restricted).

This construction allows insight into properties to be expected. First of all it is obvious that very large loops and, in particular, also loops of Polyakov type occur. Thus one can expect that the effective gauge-invariant observables resulting from gauge-variant ones become sensitive to the breaking of the $Z(2)$ symmetry. The gauge-variant propagators investigated here indeed turn out to be strongly affected by the occurring $Z(2)$ states as will be discussed in Section 4.

In the case of the propagators defined in Section 3 P contains gauge-variant terms of forms $\text{Tr}(U_{\mu x} U_{\nu y})$, $\text{Tr}(U_{\mu x} U_{\nu y}^\dagger)$ and their hermitian conjugates. By the maximizing gauge transformation then, for example, the term $\text{Tr}(U_{\mu x} U_{\nu y})$ gets the form $\text{Tr}(V_{x+e_\mu} U_{\mu x} V_x^\dagger V_{y+e_\mu} U_{\mu y} V_y^\dagger)$. The elimination procedure of V 's described above forms loops of gauge fields incorporating the U factors of these terms. In the non-abelian case because of the product form of these terms one necessarily has to connect x and y in order to eliminate all V 's. In other words, one has to form loops connecting x and y while separate loops through x and y are not possible. This has the consequence that one actually does not have correlations between separate operators, which implies that the usual transfer-matrix considerations of spectral properties do not apply.

We have performed Monte Carlo simulations on lattices of sizes $4^3 \times 8$, $8^3 \times 16$ and $16^3 \times 32$. After studies at various β the investigations to be described in Section 5 have been at large β (mainly at $\beta = 10$, some at $\beta = 99$). Similarly, after studies of transition rates between $Z(2)$ symmetry states with heat bath as well as Metropolis algorithms, for the main simulations heat bath update has been used. Measurements have been usually separated by 100 sweeps, on the small lattice also by 10 sweeps. Gauge fixing has been done iteratively site by site using the local solution (2.4) (with no V 's on the r.h.s. and with the U 's being the ones of the particular iteration step) and applying stochastic overrelaxation [12]. This iterative procedure has been stopped if $\frac{1}{4V} \sum_x \|\sum_\mu \partial_\mu^- \mathcal{O}_\mu(x)\|^2 < 10^{-8}$.

Statistical errors of observables have been determined by the jackknife method. To control the quality of gauge fixing 10 gauge copies have been generated by random gauge transformations for the configurations used in the measurements and the data

separately analyzed for the best (largest F), the first and the worst (smallest F) copy. The differences have been found to be small as compared to the statistical errors of the observables of interest, which agrees with similar observations in other investigations [7, 8, 13]. Furthermore, it has also been checked that $\Gamma_4(\tau)$ is constant within errors as it should be.

3. Forms of propagators

Let us define traceless fields $\mathcal{O}_\mu(x)$

$$\mathcal{O}_\mu(x) = \frac{1}{2i}(U_{\mu x} - U_{\mu x}^\dagger) , \quad U_{x\mu} = e^{igA_{x\mu}} , \quad (3.1)$$

and consider propagators

$$\Gamma_\mu(\vec{p}, \tau) = \frac{1}{L_4} \sum_t \text{Tr} \langle \tilde{\mathcal{O}}_\mu(\vec{p}, t + \tau) \tilde{\mathcal{O}}_\mu(-\vec{p}, t) \rangle \quad (3.2)$$

where (with $V_3 = L_1 L_2 L_3$)

$$\tilde{\mathcal{O}}_\mu(\vec{p}, \tau) = \frac{1}{V_3} \sum_{\vec{x}} e^{i\vec{p} \cdot \vec{x}} \mathcal{O}_\mu(\vec{x}, \tau) . \quad (3.3)$$

We choose $\vec{p} = (0, 0, p_3)$ (where $p_3 = \frac{2\pi}{L_3}\rho$ with integer ρ) so that the transverse components are Γ_1 and Γ_2 (in the following we use $\Gamma_T = \frac{1}{2}(\Gamma_1 + \Gamma_2)$ and analogous expressions for related quantities).

Perturbative results serve usually as a reference form in the numerical (nonperturbative) study. However, a perturbative approach in nonabelian gauge theory enclosed in a periodic box faces a problem [14, 15]. This is the zero mode problem which makes a normal perturbative expansion invalid because of the divergent gaussian integrals. These zero modes (i.e. zero-eigenvalue eigenstates of the quadratic form) are associated with zero momentum, so this problem is usually referred to as zero-momentum mode problem.

Ignoring the divergency of the gaussian integrals (which is usually the case) one arrives at the following expression for the free gluon propagator:

$$\Gamma_\mu(\vec{p}, \tau) = \frac{3g^2}{2V_4} \sum_{p_4} \frac{e^{-ip_4\tau}}{4 \sin^2 \frac{p_3}{2} + 4 \sin^2 \frac{p_4}{2}} . \quad (3.4)$$

Perturbatively the gluon is massless, and for $\vec{p} = 0$ this correlator is ill-defined.

A naive implementation of the idea of dynamical mass generation suggests to generalize eq. (3.4) as

$$\Gamma_\mu(\vec{p}, \tau) \longrightarrow \frac{3g^2}{2V_4} \sum_{p_4} \frac{e^{-ip_4\tau}}{4 \sin^2 \frac{p_3}{2} + 4 \sin^2 \frac{p_4}{2} + 4 \sinh^2 \frac{m_g}{2}} , \quad (3.5)$$

m_g being a ‘gluon mass’ (defined such that $E = m_g$ for $\vec{p} = 0$). It is usual practice to interpret all deviations from eq. (3.4) as an effect of nonzero m_g shown in eq. (3.5) (see, e.g. [1]). In this work we would like to discuss an alternative to eq.’s (3.4) and (3.5) for $\vec{p} = 0$.

There is a degeneracy of the x -independent (zero-momentum) solutions $U_{x\mu}^{cl}$ of the classical equations of motion due to the toroidal structure of the periodic lattice [16]. An example of such a solution with zero action (toron) is $U_{x\mu}^{cl} = e^{i\phi_\mu T}$, where T is one of the generators of the gauge group and ϕ_μ are four numbers. The perturbative expansion deals with fluctuations about the classical solutions (e.g. torons), and the shift $A_{x\mu}^a \rightarrow \phi_\mu + A_{x\mu}^a$ (for small fields) produces the appearance of a non-negative constant term $\sim \langle \phi_\mu^2 \rangle$ in the correlator $\Gamma_\mu(\tau)$.

To get our alternative description to eq.’s (3.4) and (3.5) we split off the zero-momentum parts

$$C_\mu = \frac{1}{V_4} \sum_x \mathcal{O}_\mu(x) \quad (3.6)$$

of the operators $\mathcal{O}_\mu(x)$ so that they decompose as

$$\tilde{\mathcal{O}}_\mu(\vec{0}, \tau) = C_\mu + \delta\tilde{\mathcal{O}}_\mu(\tau) . \quad (3.7)$$

Then eq. (3.2) for $\vec{p} = 0$ gets the form

$$\Gamma_\mu(\tau) = \text{Tr}\langle C_\mu^2 \rangle + R_\mu(\tau) ; \quad (3.8)$$

$$R_\mu(\tau) = \frac{1}{L_4} \sum_t \text{Tr}\langle \delta\tilde{\mathcal{O}}_\mu(t+\tau) \delta\tilde{\mathcal{O}}_\mu(t) \rangle . \quad (3.9)$$

Evidently,

$$\frac{1}{L_4} \sum_\tau \Gamma_\mu(\tau) = \text{Tr}\langle C_\mu^2 \rangle . \quad (3.10)$$

The first term on the r.h.s. of (3.8), being defined in terms of the original fields, can be readily determined in the Monte Carlo simulations. The term $R_\mu(\tau)$ in (3.8) describes correlations between fields $\delta\tilde{\mathcal{O}}_\mu(\tau)$ with zero-momentum parts subtracted. Making the change of variables $A_{x\mu} \rightarrow \phi_\mu + A_{x\mu}$ and using a collective-coordinate method¹ one obtains in gaussian approximation

$$\Gamma_\mu(\tau) = \text{Tr}\langle C_\mu^2 \rangle + \frac{3g^2}{2V_4} \sum_{p_4 \neq 0} \frac{e^{-ip_4\tau}}{4 \sin^2 \frac{p_4}{2}} , \quad (3.11)$$

which will be our reference form in the numerical study of the propagators $\Gamma_\mu(\tau)$.

4. Broken $Z(2)$ symmetry

To monitor the breaking of the $Z(2)$ symmetry we have measured Polyakov loops

$$P_\mu = \frac{L_\mu}{V_4} \sum_{x \neq x_\mu} \text{Tr} \prod_{x_\mu} U_{\mu x} . \quad (4.1)$$

Because of the two possibilities for each direction (i.e., $P_\mu > 0$ or $P_\mu < 0$) there are $2^4 = 16$ states : $(++++), (+++-), \dots, (----)$. Fig. 1 shows the time history of the P_μ , Γ_T and Γ_4 obtained on the $4^3 \times 8$ lattice. It is seen that the Γ_μ are, in fact, strongly affected by the indicated states and, in particular, that also the space-like

¹which works here, of course, only in lowest approximation

directions are important within this respect. The close relation between P_μ and Γ_4 is also obvious.

On larger lattices the same features are observed (though getting accurate data for illustrations by time histories gets less easy). The phenomenon occurs for all β in the deconfinement region. The transition rate between the states is smaller on larger lattices and for larger β . It depends, of course, on the algorithm which is used. For example, with heat bath updates there are considerably more transitions than with Metropolis.

From the numerical analysis we find in more detail that the observables, depending on their symmetry properties, take different values in the states. Huge differences as well as smaller differences of the values taken by the observables in different states are observed. This is seen in Fig. 2 for the example of Γ_T at finite \vec{p} on the $16^3 \times 32$ lattice (for clarity of the figure the statistical errors are not shown; they range from less than 2 % for the $(++++)$ -state to about 20 % for states with the largest magnitudes of the propagators).

It should be obvious that to obtain sensible results measurements of observables are to be done separately for each state. In particular, for comparison with usual perturbation theory only the $(++++)$ -state is appropriate. To improve statistics, instead of only selecting the $(++++)$ -data from the time history, the other configurations (solely) for the purpose of determining observables may be transformed to $(++++)$. We have checked that this leads (faster) to the same results. The $Z(2)$ transformation used, which for a particular direction leads from $-$ to $+$, is simply a factor -1 applied to the field variables of this direction (for the time direction this has already been used in Ref. [6]).

5. Zero momentum modes

We now concentrate on the $(++++)$ -state at large β , i.e. $\beta = 10$ and $\beta = 99$. To test the accuracy of the lowest order calculations we have compared numerical results for $p_3 \neq 0$ with (3.4). The deviations are generally smaller than about 10 %

and become smaller for larger β and for larger p_3 . They are certainly very small as compared to the effects to be discussed below. Thus it appears that for the present study we are sufficiently deep in the perturbative region.

For $\vec{p} = \vec{0}$ the comparison with (3.11) requires the knowledge of $\langle C_\mu^2 \rangle$ which we also determine in the Monte Carlo simulations. In addition, we obtain important properties of C_μ by comparing the time histories of C_μ , $\delta\tilde{\mathcal{O}}_\mu(\tau)$ and of

$$X_\mu(\rho) = \text{Re} \frac{1}{V_4} \sum_x e^{i\vec{p}\cdot\vec{x}} \mathcal{O}_\mu(x) \quad (5.1)$$

with $\vec{p} = (0, 0, \frac{2\pi}{L_3}\rho)$ and $\rho \neq 0$, i.e. of an example of a nonzero-momentum part of the fields.

Fig. 3 shows time histories of components C_μ^a , $\delta\tilde{\mathcal{O}}_\mu^a$ and X_μ^a (where $C_\mu = \sum_a (\sigma^a/2) C_\mu^a$ etc.). For $\delta\tilde{\mathcal{O}}_\mu^a$, $X_\mu^a(1)$ and $X_\mu^a(2)$ uniform Monte Carlo noise is seen. Its magnitude is larger if the three-momentum involved in the particular quantity gets smaller. The behavior of $\delta\tilde{\mathcal{O}}_\mu^a$, in Fig. 3 presented for $\tau = 0$, is the same for all τ . For C_μ^a in addition to noise with magnitude comparable to that of $\delta\tilde{\mathcal{O}}_\mu^a$, surprisingly large variations are observed. These variations exhibit different patterns for different μ , while for different a we find the same pattern.

A very interesting aspect of these results is that in the decomposition (3.7) of the fields $\tilde{\mathcal{O}}_\mu$ the parts C_μ^a and $\delta\tilde{\mathcal{O}}_\mu^a$ obviously behave quite differently. The observed large variations of C_μ^a appear to be a characteristic consequence of zero-momentum modes. They seem to be related to changes between different constant classical solutions as one may consider in the weak-coupling limit.

Because of the considerable size of the large variations of C_μ it is to be expected that also $\langle C_\mu^2 \rangle$ gets large as compared to other quantities. This will be seen to be indeed the case below. A further consequence of these variations is that error analyses of observables involving C_μ give unusually large errors. This, in particular holds for the propagator (3.8). In order to show that the unusually large errors are entirely due to the part $\text{Tr}\langle C_\mu^2 \rangle$ we also have measured $R_\mu(\tau)$ separately in the simulations. An example of the respective results is shown in Fig. 4. It is seen that

while $\Gamma_T(\vec{0}, \tau)$ exhibits very large errors, for $R_T(\tau)$ one indeed obtains errors of usual size.

From Fig. 4 it is obvious that our numerical results for the transverse propagator with $\vec{p} = \vec{0}$ agree reasonably well with that of our lowest-order calculation (3.11). The average over all times of the propagator is precisely $\text{Tr}\langle C_\mu^2 \rangle$ as predicted by (3.10). Analogous observations as on the $8^3 \times 16$ lattice for $\beta = 10$ have been made on the $4^3 \times 8$ lattice for $\beta = 10$ and on the $16^3 \times 32$ lattice for $\beta = 10$ and $\beta = 99$. Thus our numerical results confirm the description we have given.

To quantify the importance of zero-momentum modes we compare $\text{Tr}\langle C_\mu^2 \rangle$ with $R_\mu(0)$ (Table 1) and also with $\Gamma_\mu(\vec{p}, 0)$ with $\vec{p} \neq \vec{0}$ (Table 2). To allow for the comparison of different lattice sizes and different β the values in Tables 1 and 2 are multiplied by V_3/g^2 (which obviously cancels the extra factor implicit in our definitions as compared to usual continuum expressions). While all the other quantities then are roughly of the same order of magnitude, the values of $\text{Tr}\langle C_\mu^2 \rangle$ turn out to be much larger. From Table 1 it is seen that for increasing β this feature gets even more pronounced. The same holds for increasing lattice size. Not only ζ gets larger but there is also an increase of the ratios ζ/γ .

In literature investigations of the gluon mass have been based on determinations of effective masses $m(\tau)$ from

$$\frac{\cosh(m(\tau)(\tau + 1 - \frac{L_4}{2}))}{\cosh(m(\tau)(\tau - \frac{L_4}{2}))} = \frac{\Gamma_T(\vec{0}, \tau + 1)}{\Gamma_T(\vec{0}, \tau)}. \quad (5.2)$$

For the present data the respective results are depicted in Figure 5. Because $m(\tau)L_\mu$ shows little dependence on lattice size, these results may also be considered from the point of view of finite temperatures where screening masses are determined [7, 8]. We have shown that instead of referring to effective masses the data can perfectly be described by eq. (3.11) relying on zero-momentum modes.

6. Discussion and conclusions

To summarize, the dependence of the gauge-variant (zero momentum) propagators $\Gamma_\mu(\tau)$ on zero-momentum modes can be very strong. The mechanism of this influence can be viewed as follows. The chosen gauge fixing does not prohibit the fluctuations about some nonzero constant values $\phi_\mu^a \neq 0$, and the shift $A_{x\mu}^a \rightarrow \phi_\mu^a + A_{x\mu}^a$ (for small fields) produces the appearance of a non-negative constant term in the correlator $\Gamma_\mu(\tau) \rightarrow \text{Const} + R_\mu(\tau)$. In this paper we demonstrated the occurrence of a large constant term explicitly in the weak coupling (perturbative) limit.

Considering time histories in our simulations we have found that the zero-momentum term shows unusually large fluctuations. These fluctuations appear to be a characteristic signal for zero-momentum modes.

The question of the role of the zero-momentum modes at smaller values of β (in the physical region) needs further study. Indeed, one expects dynamical mass generation in the physical (nonperturbative) regime. However, zero-momentum modes which appear in the periodic volume may (at least, partially) mimic it, as it happens in the pure gauge $U(1)$ theory. The latter can be seen from the data in [10] as has been discussed in [9]. To disentangle these two effects, i.e. dynamically generated mass and zero-momentum mode contribution, a comparative study with different boundary conditions could be of use.

On the finite lattice at large β values one is beyond the finite-volume transitions, and thus the propagators become sensitive to the broken $Z(2)$ symmetry states of the deconfinement region usually monitored by Polyakov loops. We find here that the states signalled by the space-like Polyakov loops are important, too.

Acknowledgments

One of us (W.K.) wishes to thank M. Müller-Preussker and his group for their kind hospitality. This research was supported in part under DFG grants Ke 250/13-1 and Mu 932/1-4 and the grant INTAS-96-370.

References

- [1] J.E. Mandula and M. Ogilvie, Phys. Lett. **B185** (1987) 127.
- [2] R. Gupta, G. Guralnik, G. Kilcup, A. Patel, S.R. Sharpe and T. Warnock, Phys. Rev **D 36** (1987) 2813.
- [3] P. Marenzoni, G. Martinelli, N. Stella and M. Testa, Phys.Lett. **B318** (1993) 511; Nucl. Phys. **B455** (1995) 339.
- [4] C. Bernard, C. Parinello and A. Soni, Phys. Rev. **D 49** (1994) 1585.
- [5] A. Nakamura, H. Aiso, M. Fukuda, T. Iwamiya, T. Nakamura and M. Yoshida, YAMAGATA-HEP-95-10, hep-lat/9506024.
- [6] F. Karsch and J. Rank, Nucl.Phys. **B** (Proc. Suppl.) **42** (1995) 508.
- [7] U.M. Heller, F. Karsch and J. Rank, Phys. Lett. **B355** (1995) 511.
- [8] U.M. Heller, F. Karsch and J. Rank, FSU-SCRI-97-113, BI-TP 97/36, hep-lat/9710033.
- [9] V.K. Mitrjushkin, Phys. Lett. **B390** (1997) 293.
- [10] P. Coddington, A. Hey, J.E. Mandula and M. Ogilvie, Phys. Lett. **B197** (1987) 191.
- [11] W. Kerler, Phys. Lett. **B100** (1981) 267; Phys. Rev. **D 24** (1981)1595.
- [12] Ph. de Forcrand and R. Gupta, Nucl. Phys. **B** (Proc. Suppl.) **9** (1989) 516.
- [13] A. Cucchieri, Nucl.Phys. **B508** (1997) 353.
- [14] B.E. Baaquie, Phys. Rev. **D 16** (1977) 2612.
- [15] M. Lüscher, *Selected Topics in Lattice Field Theory*, Lectures given at Les Houches (1988), in : Fields, Strings and Critical Phenomena, ed. E. Brezin and J. Zinn-Justin (North Holland, Amsterdam, 1989).
- [16] A. Gonzales-Arroyo, J. Jurkiewicz and C.P. Korthals-Altes, Proc. 11th NATO Summer Institute, Freiburg, 1981, eds. J. Honerkamp et al. (Plenum, NY, 1982).

Table 1

$$\zeta = (V_3/g^2)\text{Tr}\langle(C_T)^2\rangle \text{ and } \gamma = (V_3/g^2)((R_T(0) - R_T(L_4/2))$$

lattice	β	ζ	γ
$4^3 \times 8$	10	6.30 (16)	1.610 (5)
$8^3 \times 16$	10	15.7 (7)	3.229 (17)
$16^3 \times 32$	10	57 (10)	6.03 (22)
$16^3 \times 32$	99	375 (86)	4.98 (19)

Table 2

$$(V_3/g^2)\Gamma_T(\vec{p}, 0) \text{ with } \vec{p} = (0, 0, \frac{2\pi}{L_3}\rho)$$

lattice	β	$\rho = 1$	$\rho = 2$	$\rho = 4$
$4^3 \times 8$	10	0.460 (2)	0.275 (1)	
$8^3 \times 16$	10	0.992 (4)	0.457 (1)	0.277 (1)
$16^3 \times 32$	10	2.100 (20)	0.981 (4)	0.457 (1)
$16^3 \times 32$	99	2.002 (23)	0.926 (5)	0.436 (2)

Figure captions

- Fig. 1. Time history of Polyakov loops and propagators (at $\tau = 0$) for $\beta = 10$ and $4^3 \times 8$ lattice.
- Fig. 2. Transverse propagators in various states for $\vec{p} = (0, 0, \frac{2\pi}{L_3})$, $\beta = 10$ and $16^3 \times 32$ lattice (curve is (3.4)).
- Fig. 3. Time histories of C_μ^a , $\delta\tilde{O}_\mu^a$, $X_\mu^a(1)$ and $X_\mu^a(2)$ for $\beta = 10$ and $16^3 \times 32$ lattice.
- Fig. 4. $\Gamma_T(\vec{0}, \tau)$ and $R_T(\tau)$ compared with (3.11) (curves) and $\text{Tr}\langle C_\mu^2 \rangle$ (constant line in upper Figure) for $\beta = 10$ and $8^3 \times 16$ lattice. Errors of R_T are smaller than symbols.
- Fig. 5. Effective masses from eq. (5.2) for $\vec{p} = \vec{0}$, $\beta = 10$ and various lattice sizes (curve based on (3.11)).

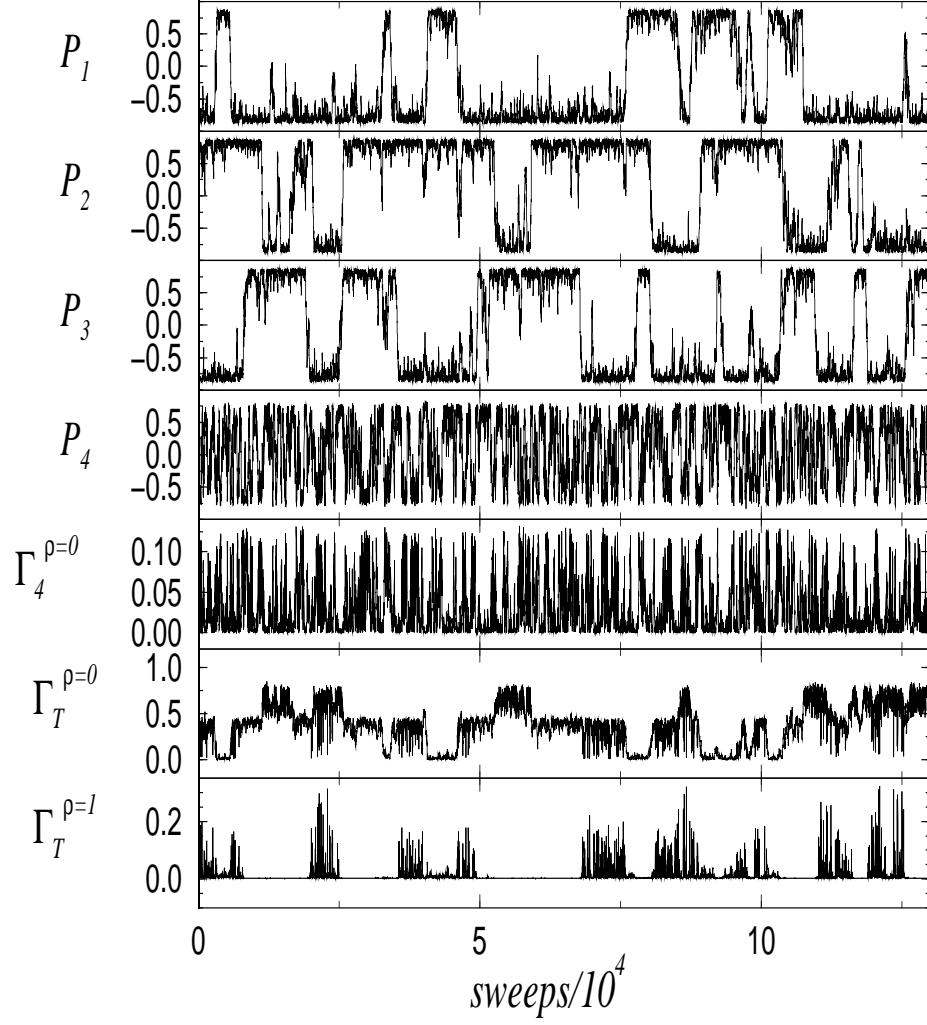


Figure 1: Time history of Polyakov loops and propagators at $\tau = 0$ for $\beta = 10$ and $4^3 \times 8$ lattice.

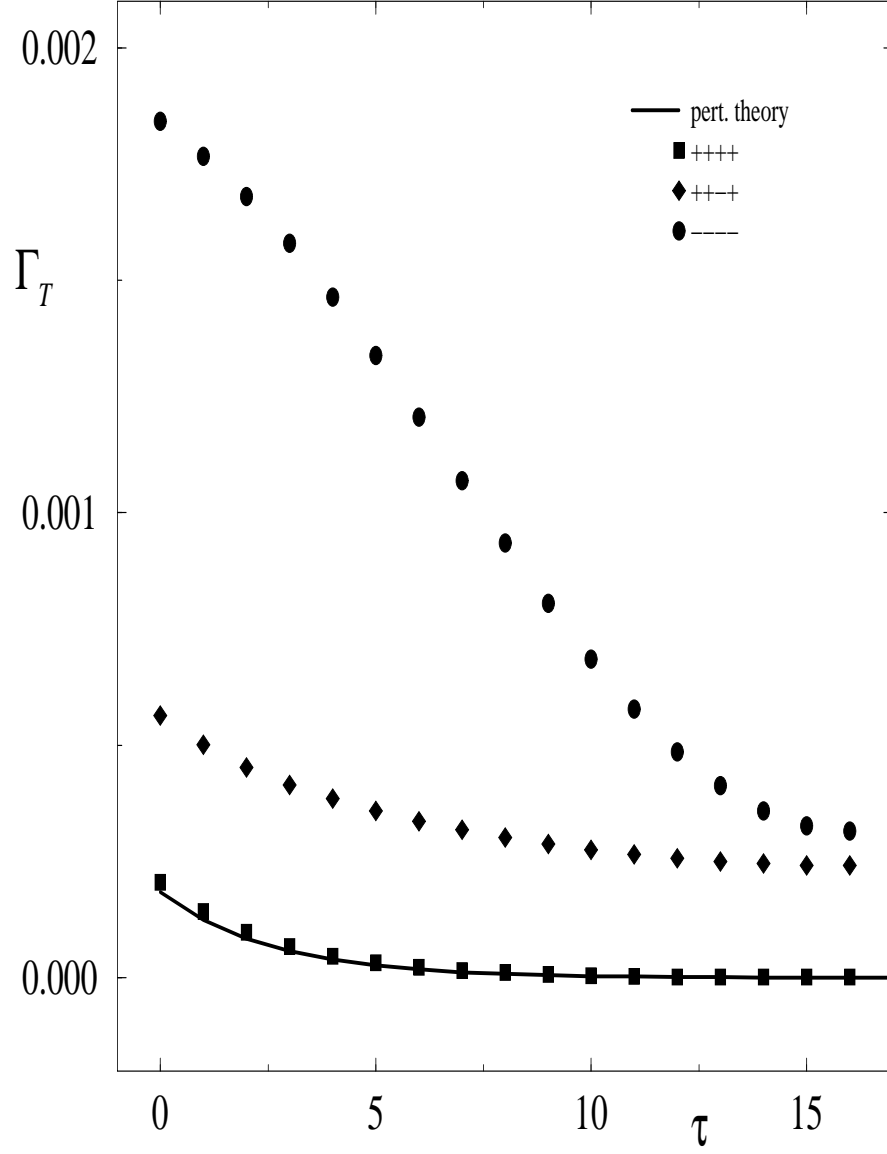


Figure 2: Transverse propagators in various states for $\vec{p} = (0, 0, \frac{2\pi}{L_3})$, $\beta = 10$ and $16^3 \times 32$ lattice (curve is (3.4)).

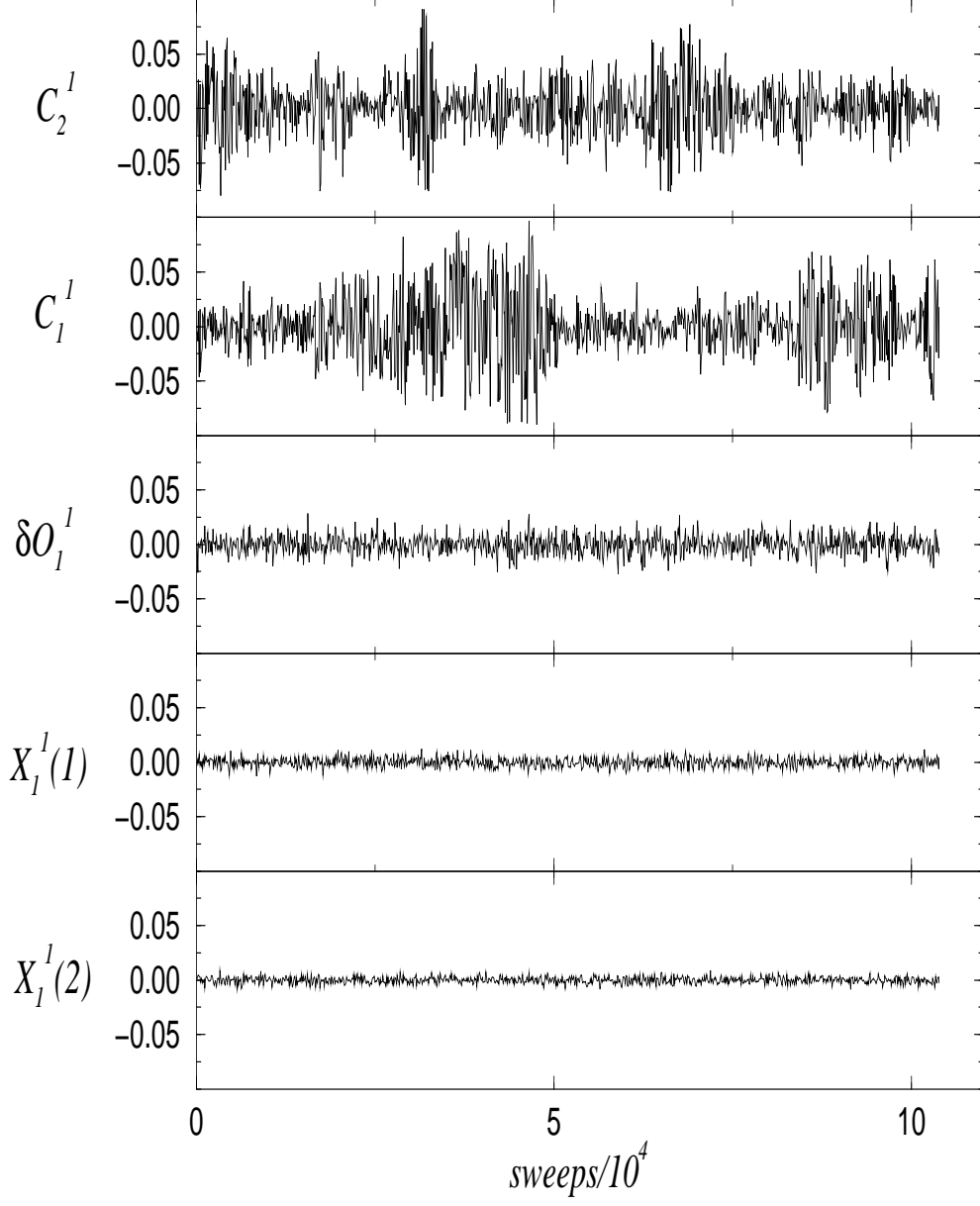


Figure 3: Time histories of C_μ^a , $\delta\tilde{O}_\mu^a$, $X_\mu^a(1)$ and $X_\mu^a(2)$ for $\beta = 10$ and $16^3 \times 32$ lattice.

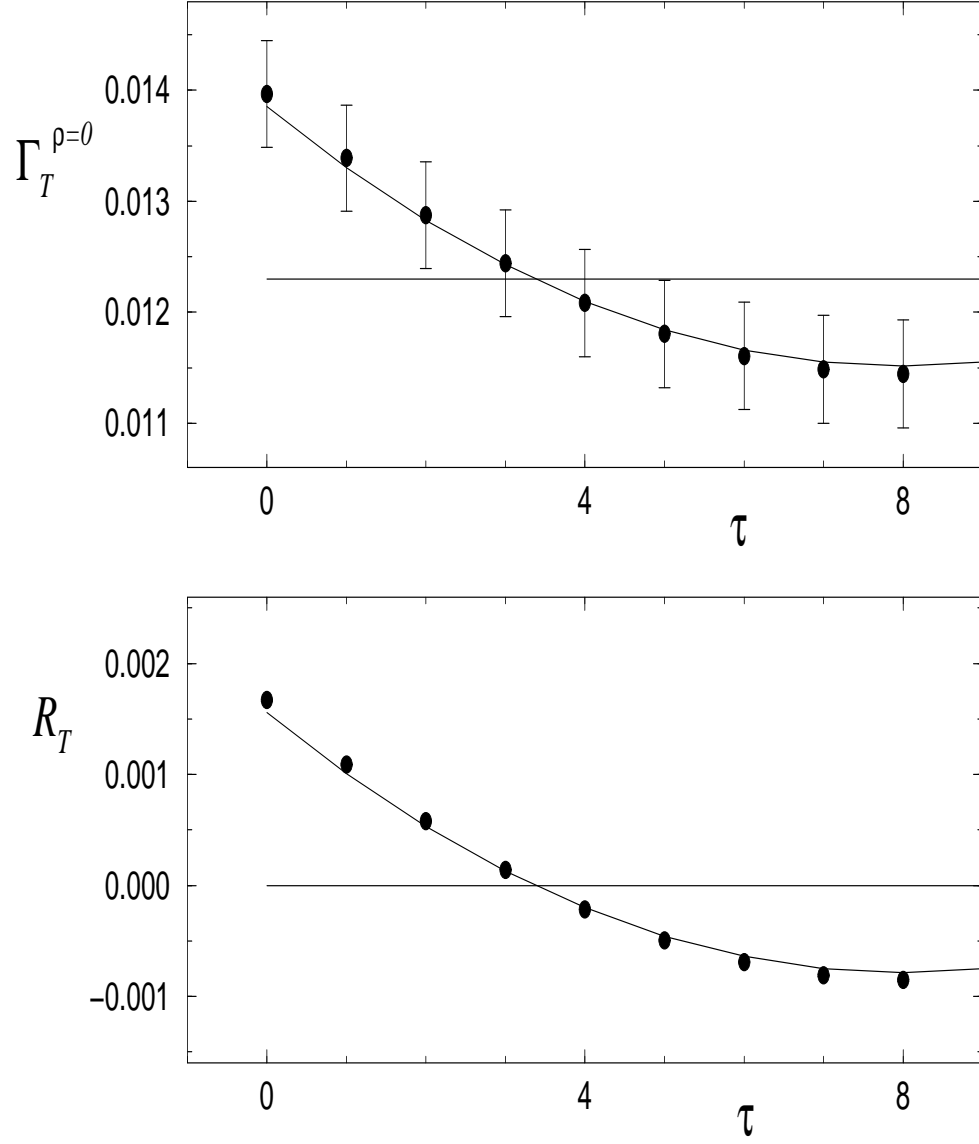


Figure 4: $\Gamma_T(\vec{0}, \tau)$ and $R_T(\tau)$ compared with (3.11) (curves) and $\text{Tr}\langle C_\mu^2 \rangle$ (constant line in upper Figure) for $\beta = 10$ and $8^3 \times 16$ lattice.

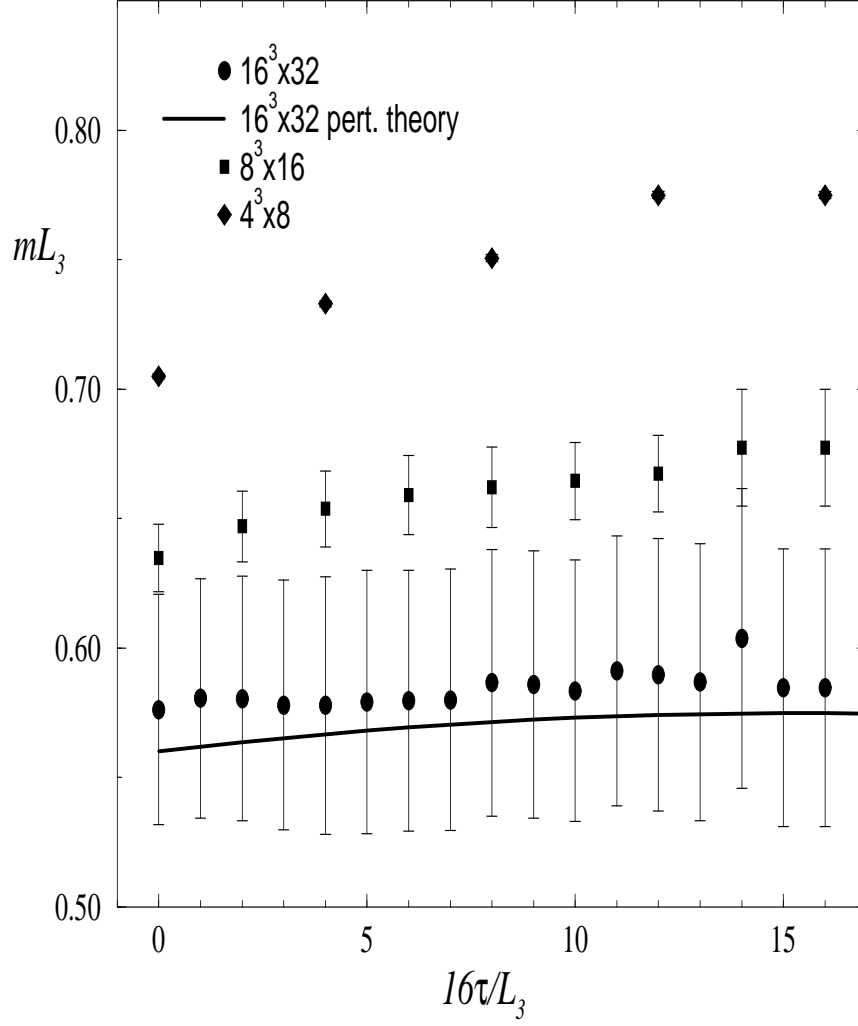


Figure 5: Effective masses from eq. (5.2) for $\vec{p} = \vec{0}$, $\beta = 10$ and various lattice sizes (curve based on (3.11)).